FRONTIERS OF PHYSICS

RESEARCH ARTICLE
Volume 18 / Issue 6 / 61303 / 2023

Single-photon source with sub-MHz linewidth for cesium-based quantum information processing

Hai He, Peng-Fei Yang, Peng-Fei Zhang, Gang Li†, Tian-Cai Zhang‡

State Key Laboratory of Quantum Optics and Quantum Optics Devices, Collaborative Innovation Center of Extreme Optics, Institute of Opto-Electronics, Shanxi University, Taiyuan 030006, China
Corresponding authors. E-mail: †gangli@sxu.edu.cn, ‡tczhang@sxu.edu.cn
Received March 27, 2023; accepted June 5, 2023

ABSTRACT

A single-photon source with narrow bandwidth, high purity, and large brightness can efficiently interact with material qubits strongly coupled to an optical microcavity for quantum information processing. Here, we experimentally demonstrate a degenerate doubly resonant single-photon source at 852 nm by the cavity-enhanced spontaneous parametric down-conversion process with a 100% duty cycle of generation. The single photon source possesses both high purity with a second-order correlation $g_h^{(2)}(0) = 0.021$ and narrow linewidth with $\Delta\nu_{sp} = (800 \pm 13)$ kHz. The single-photon source is compatible with the cesium atom D2 line and can be used for cesium-based quantum information processing.

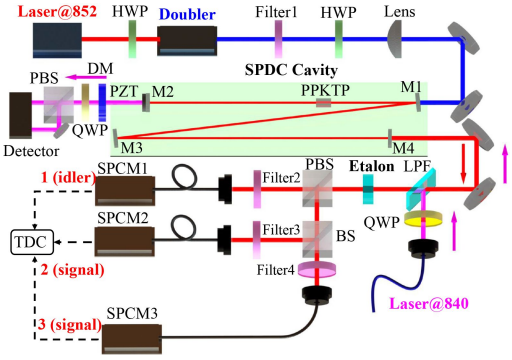

Keywords single-photon source, sub-MHz linewidth, few longitudinal modes, quantum information processing

1 Introduction

Single-photon sources, known as the basic element and the brick for structuring the building of quantum information [1], have wide applications in quantum science, such as the proof-in-principal demonstration of quantum physics [2, 3], quantum walking [4], quantum imaging [5], quantum key distribution [6], and quantum cryptography [7]. In particular, a single-photon source can also be used to generate entangled photons for long-distance quantum communication [8, 9]. Additionally, it plays important roles in quantum information processing with cavity quantum electrodynamics (QED), such as quantum communication [10], quantum computing [11, 12], quantum memory [13], and quantum networks [14, 15]. In hybrid photon-matter quantum systems, such as systems with quantum emitters strongly coupled to a cavity (such as the Fabry–Pérot (F–P) cavity [16], whispering-gallery mode (WGM) cavity [17] and fiber cavity [18]), a single-photon source possessing narrow linewidth, high purity, high brightness, and a single mode is one of the key ingredients for quantum information processing. Compared with faint laser pulses, true narrow-band single photons with perfect cavity mode matching efficiency can improve the fidelity of the controlled-NOT gate [11].

Several techniques for generating single photons have been demonstrated, for example, emission from single quantum emitters [19–25], the four-wave mixing process [26], and spontaneous parametric downconversion (SPDC) [27–29]. The SPDC is one of the most adopted methods due to its relatively simpler apparatus. Via the SPDC process, the single-photon source can be heralded by the simultaneous partner photon with a specific quantum correlation. However, the linewidth of the single-photon source from the free-space SPDC process is usually hundreds of GHz, which is several orders of magnitude larger than that of atomic transitions. The cavity-enhanced SPDC can suppress the linewidth dramatically. Several experimental groups have generated narrow-band single-photon sources at different wave-

Higher Education Press

https://doi.org/10.1007/s11467-023-1317-z

lengths by cavity-enhanced SPDC [30–34]. Narrow-band single-photon sources with several megahertz at 852 nm [35, 36] and sub megahertz at 606 nm [37], which are compatible with cesium (Cs) atomic transitions and the Pr^{3+} solid state, respectively, have been realized.

Due to the birefringence effect in cavity-enhanced SPDC with a type-II nonlinear crystal, the doubly resonant condition for both signal and idler photons is needed for the heralded single-photon source. The condition can be achieved by placing a compensation crystal [31] in the cavity, using the flip-trick technique [33], tuning the temperature of the crystal [38], and making the customized conjoined double-cavity structure [39]. However, in most experiments, the generation and measurement procedures are switched by a mechanical chopper [40, 41] and cannot guarantee a 100% duty cycle.

In this paper, we experimentally demonstrate a sub-MHz linewidth single-photon source by cavity-enhanced SPDC. With the aid of an auxiliary 840 nm laser beam, which is far from the Cs transition, to stabilize the SPDC cavity independently, a 100% duty cycle of photon generation is thus realized. By adjusting the temperature of the PPKTP (periodically poled $KTiOPO_4$), we achieve the doubly resonant condition of degenerate signal-idler photons. The generated single-photon source has a narrow linewidth of $\Delta\nu_{sp} = (800 \pm 13)$ kHz at 852 nm, very few longitudinal modes, and a fiber-coupled brightness of approximately 18 pairs/(s·mW·MHz). This single photon source with a regular spatial mode can be used for Cs-based quantum information technologies in strongly coupled cavity QED systems [8–13].

2 Experimental apparatus

Figure 1 shows the schematic of the experimental setup. An 852 nm pump laser (Toptica TA pro-850) (red) is frequency doubled to generate 426 nm light. The frequency of the pump laser is stabilized to the $F = 4 \leftrightarrow F' = 3, 5$ crossover transition between $6S_{1/2}$ and $6P_{3/2}$ of the Cs D2 line. The 426 nm light (blue) is then coupled into the SPDC cavity as pump light to generate single photons. Filter 1 (Thorlabs FESH0500, pink) is used to block the residual 852 nm light. The lens (Thorlabs AC254-200-A) before the SPDC cavity is used to match the mode waist of the SPDC cavity. Four mirrors, two flat and two concave, are arranged to form a folded F–P SPDC cavity that is more flexible for operating with a 10 mm type-Ⅱ PPKTP crystal (Raicol Crystals) inside. The 0.65 m long folded structure effectively doubles the round-trip length, and as a result, the free spectral range is approximately 224.7 MHz. All four mirrors are antireflective at 426 nm. The two concave mirrors with a curvature radius of 100 mm are highly selectively coated

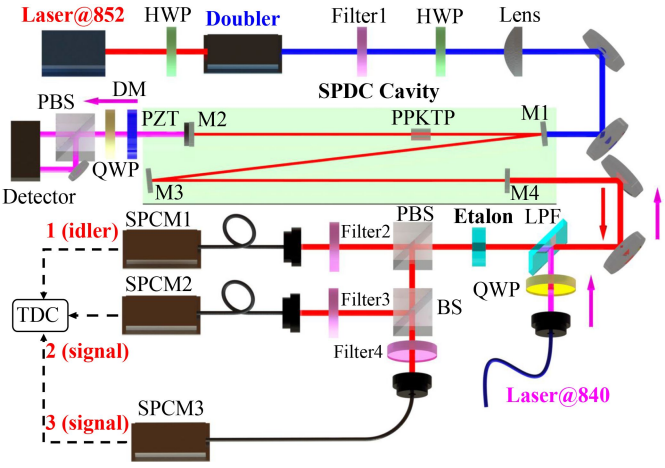

Fig. 1 Schematic of the experimental setup. A frequency-stabilized 852 nm laser is injected into a frequency doubler. The generated frequency-doubled 426 nm light is injected into the SPDC cavity. The generated signal and idler photons are separated by polarizing components and recorded by SPCMs. HWP: half-wave plate; DM: dichroic mirror; PBS: polarizing beam splitter; QWP: quarter-wave plate; PZT: piezoelectric transducers; LPF: longpass filter.

with $R > 99.99\%$ at 852 nm. The cavity mode waist is 19.6 μm at 426 nm, which is appropriately designed to optimize the conversion between the two concave mirrors. For the remaining two mirrors, one has a high reflectivity larger than 99.99% at 852 nm, and the other has a modest reflectivity (R~98%) and serves as the output coupler.

The double resonance of the generated signal and idler photons is realized by precisely tuning the temperature of the PPKTP crystal. The length of the SPDC cavity is stabilized by a piezoelectric transducer attached to one of the concave mirrors and a frequency-stabilized auxiliary 840 nm laser via the Hansch–Couillaud method [42]. A longpass filter (LPF, Semrock TLP01-887-25 × 36) is used to separate the locking beam and the SPDC cavity output signal. The generated signal and idler photons transmit an LPF and are filtered by a 3 mm long etalon to block the redundant longitudinal modes. The polarizations of the signal and idler photons are perpendicular to each other and are separated by a polarization beam splitter (PBS). The signal photons are further divided into two parts and analyzed by an HBT system [43] with a 50:50 beam splitter (BS) and two single-photon counting modules (Excelitas SPCM-850-60-FC, SPCM). The output of SPCMs is recorded by time-to-digital converters (Swabian Instruments, Time Tagger 20, TDC). Several narrow bandpass filters (Semrock LL01-852-12.5) are used to filter out the background noise.

For our 10 mm type-Ⅱ PPKTP crystal, the full width at half-maximum (FWHM) of the phase-matching spectrum [red curve in Fig. 2(a)] is approximately 300 GHz. The SPDC cavity has a length of 0.65 m with FSR ≈

225 MHz for both the signal and idler photons. The birefringence of the nonlinear crystal results in a slight difference. There are approximately 1300 modes of signal and idler photons existing within the phase-matching bandwidth of the crystal. However, the two photons are emitted only when both are resonant concurrently in the cavity. This is the so-called cluster effect [44], as shown in Fig. 2(a). Thus, the generation of photons is restricted to 3 clusters (blue lines). The purple peaks are the transmission spectrum of F–P etalon with a length of 3 mm. The overall joint function after filtering is shown in Fig. 2(b) as green peaks. The filtered field only includes approximately 3 modes in the inset.

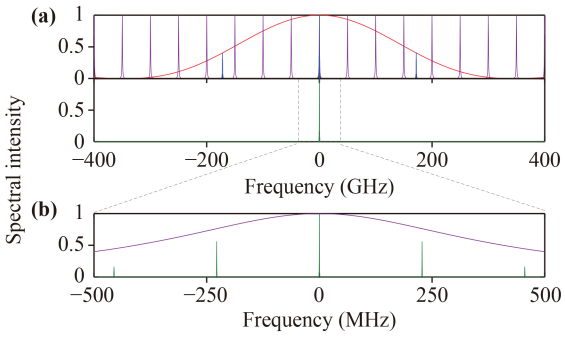

Fig. 2 Joint spectrum of generated photons. **(a)** Phase-matching spectrum of the nonlinear crystal (red curve), joint spectrum within the SPDC cavity (blue line), and transmission spectrum of the F–P filter (purple line). **(b)** The final joint spectrum of the cavity-enhanced SPDC output (green) with a 3 mm-long etalon.

3 Characterization of the single photons

Now, we characterize the generated single-photon source. Measurements of the cross-correlation between the signal and idler photons and the heralded autocorrelation function of signal photons are carried out.

3.1 The signal-idler cross correlation

The signal-idler cross correlation provides information about cavity-enhanced SPDC spectral properties such as bandwidth, number of longitudinal modes and brightness. When the SPDC cavity with a type-II crystal is double resonant to both signal and idler photons, the signal-idler cross correlation reads [45, 46]

$$g_{si}^{(2)}(\tau) \propto \left| \sum_{m_s,m_i=0}^{\infty} \frac{\sqrt{\gamma_s\gamma_i\omega_s\omega_i}}{\Gamma_s+\Gamma_i} \times \begin{cases} \mathrm{e}^{-2\pi\Gamma_s\left(\tau-\frac{\tau_0}{2}\right)}\sin c\left(\mathrm{i}\pi\tau_0\Gamma_s\right), \forall\tau \geqslant \dfrac{\tau_0}{2} \\ \mathrm{e}^{+2\pi\Gamma_i\left(\tau-\frac{\tau_0}{2}\right)}\sin c\left(\mathrm{i}\pi\tau_0\Gamma_i\right), \forall\tau < \dfrac{\tau_0}{2} \end{cases} \right|^2, \quad (1)$$

where $\Gamma_k = \frac{\gamma_k}{2} + \mathrm{i}m_k FSR_{k,eff}$ $(k \in \{s,i\})$. s and i represent the signal and idler photon, respectively. m_k is the mode index. ω_k is the central frequency. γ_k is the cavity decay rate, and τ_0 is the transmit time difference between signal and idler photons through the crystal. We have $\tau_0 = 3.92$ ps with the length of the crystal $d_0 = 10$ mm. Considering the detection system with a finite time resolution τ_D modeled by a Gaussian form of $h(t) = \sqrt{\frac{4\log 2}{\pi\tau_D^2}}\exp\left(-4\log\left(2\frac{t^2}{\tau_D^2}\right)\right)$, the convoluted cross-correlation function is then

$$\overline{g_{si}^{(2)}(\tau)} = C\int_{-\infty}^{+\infty} g_{si}^{(2)}(\tau)h(\tau-t)\mathrm{d}t. \quad (2)$$

The FWHM of the simplified cross correlation given by Eq. (2) can be approximated as $\mathrm{e}^{-2\pi\gamma|\tau|}$ with γ being the cavity decay rate, and the bandwidth of single photons is equal to $\sqrt{\sqrt{2}-1}*\gamma$ in the cavity-enhanced SPDC process [47]. When the time bin of the TDC is set to 4.4 ns, which is comparable with the time resolution of the detecting system τ_D and the round-trip time $t_{rt} = 1/\mathrm{FSR}$ of photons inside the SPDC cavity, the comb-like structure due to multiple longitudinal output modes cannot be resolved in the measured cross correlation. Figure 3 shows the measured signal-idler cross correlation versus the time delay. Here, the power of the 426 nm pump light is kept at 16 mW, and the measurement time (T_m) is set at 5 minutes. The decay rate of the cavity is extracted by exponential fitting with $\gamma = (1.25 \pm 0.02)$ MHz. The linewidth of single photons is given as $\Delta\nu_{sp} = (800 \pm 13)$ kHz, which is much smaller than the natural linewidth of the Cs D2 line.

The number of longitudinal modes can also be extracted from the explicit cross-correlation function. The FWHM of the main peak is broadened by finite time resolution τ_D, while it narrows as the number of longitudinal modes increases, as shown in Fig. 4. Figure 4(a) shows the comb-like cross correlation with different numbers of modes and a 500 ps time resolution. The purple, black, green and red solid lines correspond to the cross-correlation functions with 1-, 2-, 3- and 4-mode cases, respectively. The blue circles are the experimental data of the cross correlation with a time bin of 100 ps. The measured FWHM of the main peak, obtained by Lorenz fitting, is (0.88 ± 0.03) ns. The calculated pattern of the 3-mode case (green solid line) is in good agreement with the experimental data. Figure 4(b) provides the relationship between the FWHM of the main peak and the number of modes in the cavity with time resolutions of 0 ps (red) and 500 ps (blue). The 500 ps resolution is also adopted in the experiment. We can deduce that the number of longitudinal modes of the filtered light field is approximately 3 from the measured FWHM $= (0.88 \pm 0.03)$ ns (the green dashed lines).

The brightness and even quantumness of the source are essential for quantum information processing and are

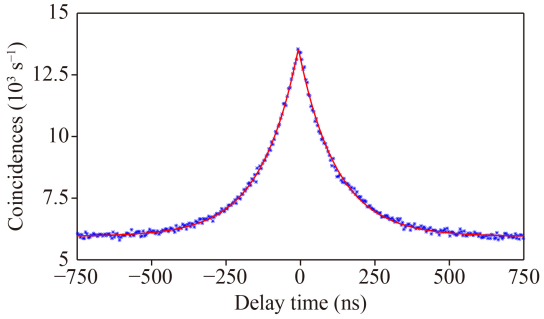

Fig. 3 The convoluted cross correlation as a function of delay time. The blue points give the measured data, and the red solid line is the fitting. The data are obtained in 5 minutes with 16 mW pump power and a 4.4 ns time bin. According to the fitting, the decay rate of the cavity is $\gamma = (1.25 \pm 0.02)$ MHz, and the corresponding bandwidth is $\Delta\nu_{sp} = (800 \pm 13)$ kHz.

shown in Fig. 5. When the pump power increases, the probability of first-order two-photon pairs increases linearly but the high-order probabilities of the multi-photon emission increase quadratically. As a result, the coincidences depend linearly on the pump power in red, while the normalized maximum of the cross-correlation function, $g_{si}^{(2)}(\max)$, is inversely proportional to the pump power in black [48]. From the black points, it is obvious that there is good quantumness with a relatively high value compared to the classical threshold of 2. When the power increases, the error bars of the coincidences increase from predominant accidental coincidences with a very large delay time. The signal-to-background ratio has a totally different trend [32]. The fiber-coupled brightness is approximately 18 pairs/(s·mW·MHz) through the linear region of the coincidences between 5 mW and 20 mW. There is a tradeoff between good quantum quality and relatively sufficient coincidences when using the source.

3.2 The second-order autocorrelation of the heralded single photons

The idler-triggered heralded second-order autocorrelation of signal photons, which describes the probability of detecting an idler-signal photon pair at time t and a second signal photon at time $t+\tau$, quantifies the purity of the single photon. This heralded autocorrelation is expressed as [33, 49]

$$g_h^{(2)}(\tau) = \frac{N_{123}(\tau)N_1}{N_{12}(0)N_{13}(\tau)}, \tag{3}$$

where $N_{12}(0), N_{13}(\tau)$, and $N_{123}(\tau)$ are the double and triple coincidence counts for detection ports 12, 13, and 123, respectively, and N_1 is the single count of idler photons. For an ideal single-photon source, the critical value of $g_h^{(2)}(0)$ should be equal to 0 at the 0 time delay

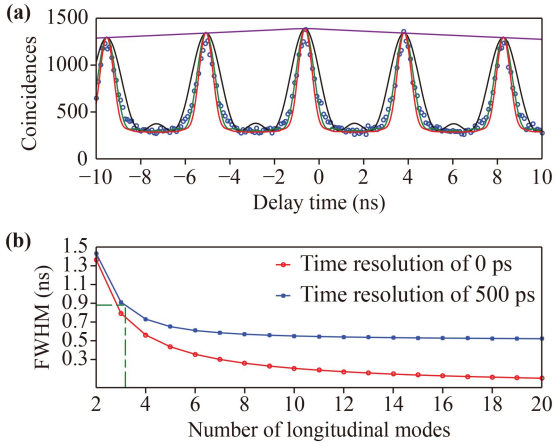

Fig. 4 The convoluted multimode cross-correlation. **(a)** The convoluted cross-correlation function in a ± 10 ns time window with a time bin of 100 ps. The FWHM of the main peak is approximately (0.88 ± 0.03) ns. **(b)** The FWHM of the main peak as a function of the number of modes N with a 10 mm long type-II PPKTP crystal. Under the condition of $\tau_D = 500$ ps (blue line), the FWHM decreases when N increases. The result with $\tau_D = 0$ ps (red line) is also shown for comparison. The numerical values $FSR = 224.7$ MHz and $\gamma_s = \gamma_i = 1.25$ MHz are used for the calculation. The effective mode number of our experiment is between 3 and 4, as shown by the green dashed line.

dependent on the pump power [50]. As long as $g_h^{(2)}(0) < 0.5$, the probability of a single photon is much lower than the multiphoton probability, and the measured light can be seen as a single-photon source.

We measure the heralded autocorrelation at the 0 time delay with a series of powers of 426 nm light. The results are shown in Fig. 6, where the error bars are given by $g_{err}(\tau) = g_h^{(2)}(\tau) \cdot \sqrt{\frac{1}{N_1} + \frac{1}{N_{123}(\tau)} + \frac{1}{N_{12}(0)} + \frac{1}{N_{13}(\tau)}}$. The green line with $g_h^{(2)}(0) = 0.5$ gives the boundary of the single-photon source. In the measurement, we keep the appropriate coincidence window (120 ns). The pump

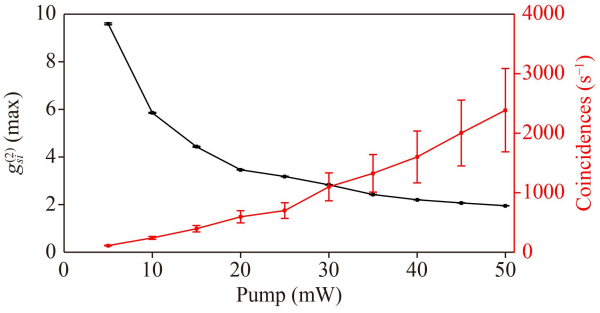

Fig. 5 The normalized maximum of the cross-correlation, $g_{si}^{(2)}(\max)$, versus the pump power is plotted in the black points on the left axis. On the right axis, the coincidences as a function of the power are shown in the red points. When the pump power decreases, a stronger bunching effect between signal-idler pairs can be observed and the signal-to-background ratio improves.

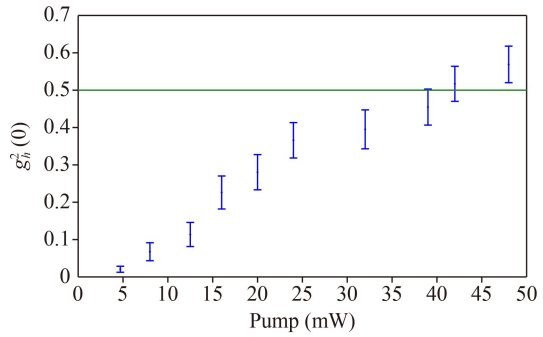

Fig. 6 The dependence of heralded autocorrelation $g_h^{(2)}(0)$ as a function of the pump power. The measured $g_h^{(2)}(0)$ is less than 0.5 depending on the power up to 40 mW. The green line is the boundary of $g_h^{(2)}(0) = 0.5$.

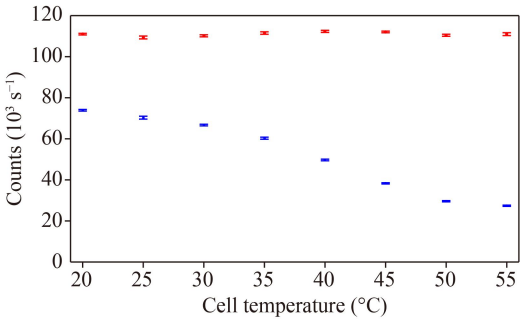

Fig. 7 The transmitted counts of the signal photons (blue points) as a function of the temperatures through a Cs vapor cell. When temperatures increase, the transmitted counts decrease. As a comparison, the counts of idler photons (red points) remain unchanged in the process.

power is varied from 4.7 mW to 48 mW. The minimum value of heralded autocorrelation is obtained with $g_h^{(2)}(0) = 0.021 \pm 0.008$ at a pump power of 4.7 mW. As the pump power increases, the measured heralded autocorrelation $g_h^{(2)}(0)$ becomes larger. When the power is smaller than 40 mW, the obtained field can be seen as a single-photon source.

3.3 The interaction between single photons and Cs atoms

To test the compatibility between the SPDC source and the atomic system [36, 51], we tune the frequency of generated photons to $F = 4 \leftrightarrow F' = 5$ and measure the transmittance of the signal photons in blue points through a 5 cm long Cs vapor cell at different temperatures, as shown in Fig. 7. The transmitted counts decrease when the temperature of the cell increases, which results in the increasing density of the cesium atoms. Up to 63% of photons can interact with Cs atoms at 55 °C. In the whole measurement, the counts of idler photons in red points remain almost constant as the reference.

4 Conclusion

In conclusion, we have experimentally demonstrated a narrow-band single-photon source by the cavity-enhanced SPDC method, where a folded F–P SPDC cavity is elaborately designed that is resonant to both signal and idler photons simultaneously. An independent laser beam is used to lock the cavity, which makes a 100% duty cycle of photon generation. A heralded autocorrelation with a minimum value of $g_h^{(2)}(0) = 0.021 \pm 0.008$ and a pump power of 4.7 mW is experimentally obtained. The linewidth is $\Delta\nu_{sp} = (800 \pm 13)$ kHz, and the fiber-coupled brightness is approximately 18 pairs/(s·mW·MHz). The brightness can be improved by adding a compensation crystal into the SPDC cavity to achieve double resonance of the signal and idler photon in further experiments. To improve the interaction strength between a single-photon source and cesium atoms in a single-mode operation, we can replace an F–P etalon narrow linewidth or pass through a cesium vapor cell which acts as an atom-based filter. The single-photon source has a wavelength of 852 nm, and the frequency can be freely tuned to match different cesium hyperfine transitions in the D2 line. The single photon source can be used for Cs-based quantum information processing.

Declarations The authors declare that they have no competing interests and there are no conflicts.

Availability of data and material The data that support the findings of this study are available from the corresponding author, upon reasonable request.

Acknowledgements This work was supported by the National Natural Science Foundation of China (Grant Nos. 11974223, and 11974225), and the Fund for Shanxi 1331 Project Key Subjects Construction.

References

1. E. Knill, R. Laflamme, and G. J. Milburn, A scheme for efficient quantum computation with linear optics, *Nature* 409(6816), 46 (2001)
2. N. Piro, F. Rohde, C. Schuck, M. Almendros, J. Huwer, J. Ghosh, A. Haase, M. Hennrich, F. Dubin, and J. Eschner, Heralded single- photon absorption by a single atom, *Nat. Phys.* 7(1), 17 (2011)
3. V. Jacques, E. Wu, F. Grosshans, F. Treussart, P. Grangier, A. Aspect, and J. F. Roch, Experimental realization of Wheeler's delayed-choice Gedanken experiment, *Science* 315(5814), 966 (2007)
4. C. Esposito, M. R. Barros, A. Durán Hernández, G. Carvacho, F. Di Colandrea, R. Barboza, F. Cardano, N. Spagnolo, L. Marrucci, and F. Sciarrino, Quantum

walks of two correlated photons in a 2D synthetic lattice, *NPJ Quantum Inf.* 8(1), 34 (2022)
5. T. B. Pittman, Y. H. Shih, D. V. Strekalov, and A. V. Sergienko, Optical imaging by means of two-photon quantum entanglement, *Phys. Rev. A* 52(5), R3429 (1995)
6. Y. F. Yan, L Zhou, W Zhong, and Y. B. Sheng, Measurement-device-independent quantum key distribution of multiple degrees of freedom of a single photon, *Front. Phys.* 16(1), 11501 (2021)
7. A. Beveratos, R. Brouri, T. Gacoin, A. Villing, J. P. Poizat, and P. Grangier, Single photon quantum cryptography, *Phys. Rev. Lett.* 89(18), 187901 (2002)
8. L. M. Duan, M. D. Lukin, J. I. Cirac, and P. Zoller, Long-distance quantum communication with atomic ensembles and linear optics, *Nature* 414(6862), 413 (2001)
9. J. Yin, Y. Cao, Y. H. Li, S. K. Liao, L. Zhang, et al., Satellite-based entanglement distribution over 1200 kilometers, *Science* 356(6343), 1140 (2017)
10. M. Brekenfeld, D. Niemietz, J. D. Christesen, and G. Rempe, A quantum network node with crossed optical fibre cavities, *Nat. Phys.* 16(6), 647 (2020)
11. A. Reiserer, N. Kalb, G. Rempe, and S. Ritter, A quantum gate between a flying optical photon and a single trapped atom, *Nature* 508(7495), 237 (2014)
12. S. Daiss, S. Langenfeld, S. Welte, E. Distante, P. Thomas, L. Hartung, O. Morin, and G. Rempe, A quantum-logic gate between distant quantum-network modules, *Science* 371(6529), 614 (2021)
13. S. Langenfeld, O. Morin, M. Korber, and G. Rempe, A network-ready random-access qubits memory, *npj Quantum Inf.* 6(1), 86 (2020)
14. H. J. Kimble, The quantum internet, *Nature* 453(7198), 1023 (2008)
15. S. Ritter, C. Nolleke, C. Hahn, A. Reiserer, A. Neuzner, M. Uphoff, M. Mucke, E. Figueroa, J. Bochmann, and G. Rempe, An elementary quantum network of single atoms in optical cavities, *Nature* 484(7393), 195 (2012)
16. J. T. Sheng, Y. X. Chao, S. Kumar, H. Q. Fan, J. Sedlacek, and J. P. Shaffer, Intracavity Rydberg-atom electromagnetically induced transparency using a high-finesse optical cavity, *Phys. Rev. A* 96(3), 033813 (2017)
17. C. Junge, D. O'Shea, J. Volz, and A. Rauschenbeutel, Strong coupling between single atoms and nontransversal photons, *Phys. Rev. Lett.* 110(21), 213604 (2013)
18. S. Kato and T. Aoki, Strong coupling between a trapped single atom and an all-fiber cavity, *Phys. Rev. Lett.* 115(9), 093603 (2015)
19. J. McKeever, A. Boca, A. D. Boozer, R. Miller, J. R. Buck, A. Kuzmich, and H. J. Kimble, Deterministic generation of single photons from one atom trapped in a cavity, *Science* 303(5666), 1992 (2004)
20. B. Liu, G. Jin, J. He, and J. M. Wang, Suppression of single-cesium atom heating in a microscopic optical dipole trap for demonstration of an 852-nm triggered single-photon source, *Phys. Rev. A* 94(1), 013409 (2016)
21. B. Darquié, M. P. A. Jones, J. Dingjan, J. Beugnon, S. Bergamini, Y. Sortais, G. Messin, A. Browaeys, and P. Grangier, Controlled single-photon emission from a single trapped two-level atom, *Science* 309(5733), 454 (2005)
22. G. Stein, V. Bushmakin, Y. J. Wang, A. W. Schell, and I. Gerhardt, Narrow-band fiber-coupled single-photon source, *Phys. Rev. Appl.* 13(5), 054042 (2020)
23. M. Keller, B. Lange, K. Hayasaka, W. Lange, and H. Walther, Continuous generation of single photons with controlled waveform in an ion-trap cavity system, *Nature* 431(7012), 1075 (2004)
24. C. Y. Lu and J. W. Pan, Quantum-dot single-photon sources for the quantum internet, *Nat. Nanotechnol.* 16(12), 1294 (2021)
25. E. Togan, Y. Chu, A. S. Trifonov, L. Jiang, J. Maze, L. Childress, M. V. G. Dutt, A. S. Sorensen, P. R. Hemmer, A. S. Zibrov, and M. D. Lukin, Quantum entanglement between an optical photon and a solid-state spin qubit, *Nature* 466(7307), 730 (2010)
26. K. B. Dideriksen, R. Schmieg, M. Zugenmaier, and E. S. Polzik, Room-temperature single-photon source with near-millisecond built-in memory, *Nat. Commun.* 12(1), 3699 (2021)
27. A. I. Lvovsky, H. Hansen, T. Aichele, O. Benson, J. Mlynek, and S. Schiller, Quantum state reconstruction of the single- photon Fock state, *Phys. Rev. Lett.* 87(5), 050402 (2001)
28. V. Prakash, L. C. Bianchet, M. T. Cuairan, P. Gomez, N. Bruno, and M. W. Mitchell, Narrowband photon pairs with independent frequency tuning for quantum light–matter interactions, *Opt. Express* 27(26), 38463 (2019)
29. J. S. Tang, L. Tang, H. D. Wu, Y. Wu, H. Sun, H. Zhang, T. Li, Y. Q. Lu, M. Xiao, and K. Xia, Towards on-demand heralded single-photon sources via photon blockade, *Phys. Rev. Appl.* 15(6), 064020 (2021)
30. K. Wakui, H. Takahashi, A. Furusawa, and M. Sasaki, Photon subtracted squeezed states generated with periodically poled $KTiOPO_4$, *Opt. Express* 15(6), 3568 (2007)
31. M. Scholz, L. Koch, and O. Benson, Statistics of narrow-band single photons for quantum memories generated by ultrabright cavity-enhanced parametric down-conversion, *Phys. Rev. Lett.* 102(6), 063603 (2009)
32. Z. Y. Zhou, D. S. Ding, Y. Li, F. Y. Wang, and B. S. Shi, Cavity-enhanced bright photon pairs at telecom wavelengths with a triple-resonance configuration, *J. Opt. Soc. Am. B* 31(1), 128 (2014)
33. M. Rambach, A. Nikolova, T. J. Weinhold, and A. G. White, Sub-megahertz linewidth single photon source, *APL Photonics* 1(9), 096101 (2016)
34. K. Niizeki, K. Ikeda, M. Y. Zheng, X. P. Xie, K. Okamura, N. Takei, N. Namekata, S. Inoue, H. Kosaka, and T. Horikiri, Ultrabright narrow-band telecom two-photon source for long-distance quantum communication, *Appl. Phys. Express* 11(4), 042801 (2018)
35. A. Moqanaki, F. Massa, and P. Walther, Novel single-mode narrow-band photon source of high brightness tuned to cesium D2 line, *APL Photonics* 4(9), 090804 (2019)
36. P. J. Tsai and Y. C. Chen, Ultrabright, narrow-band photon-pair source for atomic quantum memories, *Quantum Sci. Technol.* 3(3), 034005 (2018)

37. J. Liu, J. Liu, P. Yu, and G. Zhang, Sub-megahertz narrow-band photon pairs at 606 nm for solid-state quantum memories, *APL Photonics* 5(6), 066105 (2020)
38. L. Tian, S. J. Li, H. X. Yuan, and H. Wang, Generation of narrow-band polarization-entangled photon pairs at a rubidium D1 line, *J. Phys. Soc. Jpn.* 85(12), 124403 (2016)
39. J. Wang, Y. F. Huang, C. Zhang, J. M. Cui, Z. Y. Zhou, B. H. Liu, Z. Q. Zhou, J. S. Tang, C. F. Li, and G. C. Guo, Universal photonic quantum interface for a quantum network, *Phys. Rev. Appl.* 10(5), 054036 (2018)
40. H. Zhang, X. M. Jin, J. Yang, H. N. Dai, S. J. Yang, T. M. Zhao, J. Rui, Y. He, X. Jiang, F. Yang, G. S. Pan, Z. S. Yuan, Y. Deng, Z. B. Chen, X. H. Bao, S. Chen, B. Zhao, and J. W. Pan, Preparation and storage of frequency-uncorrelated entangled photons from cavity-enhanced spontaneous parametric downconversion, *Nat. Photonics* 5(10), 628 (2011)
41. J. Fekete, D. Rieländer, M. Cristiani, and H. de Riedmatten, Ultranarrow-band photon-pair source compatible with solid state quantum memories and telecommunication networks, *Phys. Rev. Lett.* 110(22), 220502 (2013)
42. T. W. Hansch and B. Couillaud, Laser frequency stabilization by polarization spectroscopy of a reflecting reference cavity, *Opt. Commun.* 35(3), 441 (1980)
43. R. H. Brown and R. Q. Twiss, Correlation between photons in two coherent beams of light, *Nature* 177(4497), 27 (1956)
44. C. S. Chuu, G. Y. Yin, and S. E. Harris, A miniature ultrabright source of temporally long, narrowband biphotons, *Appl. Phys. Lett.* 101(5), 051108 (2012)
45. M. Scholz, L. Koch, and O. Benson, Analytical treatment of spectral properties and signal-idler intensity correlations for a double-resonant optical parametric oscillator far below threshold, *Opt. Commun.* 282(17), 3518 (2009)
46. F. Wolfgramm, Y. A. de Icaza Astiz, F. A. Beduini, A. Cerè, and M. W. Mitchell, Atom-resonant heralded single photons by interaction-free measurement, *Phys. Rev. Lett.* 106(5), 053602 (2011)
47. Y. J. Lu and Z. Y. Ou, Optical parametric oscillator far below threshold: Experiment versus theory, *Phys. Rev. A* 62(3), 033804 (2000)
48. M. Wahl, T. Röhlicke, H. J. Rahn, R. Erdmann, G. Kell, A. Ahlrichs, M. Kernbach, A. W. Schell, and O. Benson, Integrated multichannel photon timing instrument with very short dead time and high throughput, *Rev. Sci. Instrum.* 84(4), 043102 (2013)
49. M. Beck, Comparing measurements of $g^{(2)}(0)$ performed with different coincidence detection techniques, *J. Opt. Soc. Am. B* 24(12), 2972 (2007)
50. U. Paudel, J. J. Wong, M. Goggin, P. G. Kwiat, A. S. Bracker, M. Yakes, D. Gammon, and D. G. Steel, Direct excitation of a single quantum dot with cavity-SPDC photons, *Opt. Express* 27(11), 16308 (2019)
51. C. H. Wu, T. Y. Wu, Y. C. Yeh, P. H. Liu, C. H. Chang, C. K. Liu, T. Cheng, and C. S. Chuu, Bright single photons for light–matter interaction, *Phys. Rev. A* 96(2), 023811 (2017)